Two-Dimensional Platform for Networks of Majorana Bound States

Michael Hell,[1,2] Martin Leijnse,[1,2] and Karsten Flensberg[1]
[1]Center for Quantum Devices and Station Q Copenhagen, Niels Bohr Institute, University of Copenhagen, DK-2100 Copenhagen, Denmark
[2]Division of Solid State Physics and NanoLund, Lund University, Box 118, S-22100 Lund, Sweden
(Received 5 September 2016; published 10 March 2017)

We model theoretically a two-dimensional electron gas (2DEG) covered by a superconductor and demonstrate that topological superconducting channels are formed when stripes of the superconducting layer are removed. As a consequence, Majorana bound states (MBSs) are created at the ends of the stripes. We calculate the topological invariant and energy gap of a single stripe, using realistic values for an InAs 2DEG proximitized by an epitaxial Al layer. We show that the topological gap is enhanced when the structure is made asymmetric. This can be achieved either by imposing a phase difference (by driving a supercurrent or using a magnetic-flux loop) over the strip or by replacing one superconductor by a metallic gate. Both strategies also enable control over the MBS splitting, thereby facilitating braiding and readout schemes based on controlled fusion of MBSs. Finally, we outline how a network of Majorana stripes can be designed.

DOI: 10.1103/PhysRevLett.118.107701

Majorana bound states (MBSs) are states localized at the edges of topological superconductors [1–4]. They have nonlocal properties that may be utilized for storage and manipulation of quantum information in a topologically protected way [5–7]. However, the realization of MBSs requires superconducting p-wave pairing, which appears only in exotic materials. Therefore, there is currently a search for ways to engineer p-wave pairing by combining s-wave superconductors with strong spin-orbit materials. Recent experiments looked for evidence of MBSs in, for example, semiconducting nanowires [8–14], topological insulators [15], and magnetic atom chains [16,17]. These systems may also allow demonstration experiments of the nonlocal properties of MBSs, for example, using recent suggestions for controlling MBSs in prototypical architectures [18–23]. However, to go beyond basic demonstration experiments, a scalable and flexible platform for large-scale MBS networks is needed.

Here, we suggest one such flexible platform based on a two-dimensional electron gas (2DEG) with strong spin-orbit coupling in proximity to a superconductor [24]. Such structures, reviewed in Ref. [25], have been realized by contacting InAs surface inversion layers [26,27] or InAs/InGaAs heterostructures [28,29] with superconducting Nb or Al. Recently, it has become possible to grow an Al top layer epitaxially [24], forming a clean interface with the 2DEG. The proximitized 2DEG (denoted by pS) develops a hard superconducting gap as revealed by experiments on pS-N quantum point contacts [30] or gateable pS-N-pS junctions [24] with clear signatures of multiple Andreev reflection [31] and nontrivial Fraunhofer patterns [32]. The transport properties of these structures have been studied extensively [25], but their potential as a MBS platform has not.

We show how to design and control MBSs in a pS system with a stripe of the superconducting layer removed to form an effective one-dimensional topological superconductor. This forms a pS-N-pS junction as sketched in Fig. 1(a), which can be fabricated by standard lithographic techniques. We show, similar to other semiconductor-based setups [33–37], that this system undergoes several topological phase transitions when increasing a magnetic field parallel to the stripe for parameters readily available in the lab. We base our findings on a numerical tight-binding calculation of the energy spectrum, the topological invariant, as well as transport calculations [38]. We discuss how

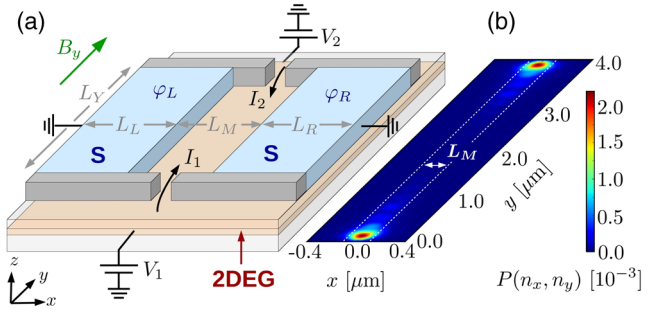

FIG. 1. Illustration of a stripe hosting MBSs in a 2DEG-based platform. Panel (a) shows the device with the superconducting layer removed along a stripe, and point contacts formed at the ends to facilitate tunneling spectroscopy of the MBSs shown in (b), where the probability density [38] $P(n_x, n_y)$ of the MBS wave function is plotted. The calculation is done on a lattice with $N_x = 260$ and $N_y = 160$ sites, and the parameters are $E_Z = 200$ μeV, $\Gamma_L = \Gamma_R = 180$ μeV, $\alpha = 1.42 \times 10^{-4}c$, $\mu = 0$, $L_L = L_R = 1$ μm, $L_M = 250$ nm, $L_Y = 4$ μm, $m^* = 0.023m_e$, and $\varphi_L = \varphi_R = 0$.

the topological energy gap depends on various parameters, which is vital for the topological protection and the manipulation time scales of the MBSs. We show that two slight modifications of the structure shown in Fig. 1, which break the inversion symmetry, give a large enhancement of the topological gap: (i) a phase bias (generated by a supercurrent) across the stripe or (ii) a replacement of one of the superconducting top layers by a gate electrode. Both methods allow us to fuse the MBS electrically, which can be used to manipulate MBSs in 2DEG structures. In the last part of the Letter, we discuss designs of more advanced MBS networks for fusion-rule testing and braiding.

Model.—We model the (unproximitized) 2DEG by a single electron band with effective mass m^* and electrochemical potential μ. The device has a finite extension with $-(L_L + L_M/2) \le x \le (L_R + L_M/2)$ and $|y| \le L_Y/2$, where it is described by the Bogoliubov–de Gennes Hamiltonian ($e = \hbar = k_B = c = 1$):

$$H(x,y) = \left[-\frac{1}{2m^*}(\partial_x^2 + \partial_y^2) - \mu\right]\tau_z - i\alpha(\sigma_x\partial_y - \sigma_y\partial_x)\tau_z + E_Z\sigma_y/2. \quad (1)$$

In the second line, we add the Rashba spin-orbit coupling (with velocity α) and the Zeeman energy (E_Z) due to a magnetic field along the stripe. The Hamiltonian acts on the four-component spinor $\psi = [\psi_{e,\uparrow}, \psi_{e,\downarrow}, \psi_{h,\downarrow}, -\psi_{h,\uparrow}]^T$ containing the electron (e) and hole (h) components for spin $\sigma = \uparrow, \downarrow$. The Pauli matrices τ_i and σ_i ($i = x, y, z$) act on the particle-hole and spin space, respectively.

We include the proximity effect of the superconducting top layer within the Green's function formalism. Integrating out the superconductor in the wideband limit, the Green's function of the 2DEG reads [49–51]

$$G_R(x,\omega) = [\omega - H(x,y) - \Sigma(x,\omega) + i0_+]^{-1}, \quad (2)$$

with self-energy for $\omega < \Delta$

$$\Sigma(x,\omega) = \Gamma(x)\frac{\Delta[\cos\varphi(x)\tau_x - \sin\varphi(x)\tau_y] - \omega}{\sqrt{\Delta^2 - (\omega + i0)^2}}. \quad (3)$$

The self-energy is zero in the stripe region, $\Gamma(|x| < L_M/2) = 0$, and nonzero under the two superconducting layers coupled to the 2DEG with symmetric tunneling rates, $\Gamma(|x| > L_M/2) = \Gamma$. In this way, we make an assumption about only the superconducting order parameter in the metallic top layer, while the superconducting pairing in the 2DEG is determined by Eq. (2). The two top layers are assumed to have the same gap Δ but possibly different phases $\varphi(x < -L_M/2) = \varphi_L$ and $\varphi(x > L_M/2) = \varphi_R$. Such a phase bias can be realized experimentally by running a supercurrent across the stripe. Our self-energy does not include a proximity-induced shift of the chemical potential under the superconductor. This is motivated by recent experiments [31] showing that pS-N-pS junctions have a high transparency, which indicates a rather small mismatch in Fermi velocities.

Symmetry class and topological invariants.—We first investigate the general topological properties of the stripe. Since its aspect ratio is large ($L_Y \gg L_M$), the system is quasi-1D, similar to coupled [52,53] or multiband [50,54] nanowires. The topological properties are, in general, determined by the zero-frequency Green's function $G^R(x,0)$ [55,56]. The self-energy $\Sigma(x,0)$ takes in this limit the form of a nondissipative pairing term, and the topological properties are thus determined by [57]

$$H_{\text{eff}} = H(x,y) + \Gamma(x)[\cos\varphi(x)\tau_x - \sin\varphi(x)\tau_y]. \quad (4)$$

This effective Hamiltonian respects particle-hole symmetry, since it anticommutes with the antiunitary operator $P = \sigma_y\tau_y\mathcal{K}$ ($\mathcal{K}$ denotes the complex conjugation). If no generalized time-reversal symmetry is present, the system is thus in symmetry class D ($P^2 = 1$) with a $\mathbb{Z}_2$ topological invariant $W_{\mathbb{Z}_2}$ [58,59].

However, our system can also be in the higher-symmetry class BDI with an integer topological invariant $W_{\mathbb{Z}}$. This is the case if the system has spatial symmetry in the x direction ($L_L = L_R$), assuming here no disorder in the x direction. The effective Hamiltonian then possesses an additional generalized "time-reversal" symmetry: It commutes with the antiunitary operator $T = \sigma_z I_x\mathcal{K}$ (I_x is the reflection in the x direction) [60]. This symmetry holds even in the presence of a phase bias [61]. Unlike the physical time reversal, the generalized operator T squares to identity, $T^2 = 1$. If both P and T symmetry are present, chiral symmetry is also present; i.e., H_{eff} anticommutes with $C = -iPT = \sigma_x\tau_y I_x$.

To predict a topological phase transition, we compute topological invariants $W_{\mathbb{Z}}$ (BDI) and $W_{\mathbb{Z}_2}$ (D). To obtain $W_{\mathbb{Z}}$, we follow Ref. [62]: Because the chirality operator satisfies $C^\dagger C = C^2 = 1$, its only eigenvalues are ± 1 and in these two subblocks the Hamiltonian is off-diagonal (since $[C, H_{\text{eff}}]_+ = 0$):

$$C = \begin{pmatrix} 1 & 0 \\ 0 & -1 \end{pmatrix}, \qquad H_{\text{eff}} = \begin{pmatrix} 0 & A \\ A^\dagger & 0 \end{pmatrix}. \quad (5)$$

The $\mathbb{Z}$ invariant follows from the winding number of the phase $\theta(k_y)$ of the determinant of A, $\det A(k_y)/|\det A(k_y)| = e^{i\theta(k_y)}$ as $W_{\mathbb{Z}} = \int_0^\infty dk_y d\theta(k_y)/dk_y/\pi$. The integer $W_{\mathbb{Z}}$ characterizes the number of MBSs which appear at the boundaries of a long stripe with two topologically trivial regions.

When T symmetry is broken, an even number of MBSs on the same boundary couple to each other, turning them into finite-energy modes. This leaves either zero or one MBS, characterized by the $\mathbb{Z}_2$ invariant $W_{\mathbb{Z}_2}$. We compute

$W_{\mathbb{Z}_2}$ in the standard way [63] by representing $H_{\rm eff}$ as a matrix $M(k_y)$ in the Majorana representation. The topological invariant is given by the relative sign of the Pfaffian of $M(k_y)$ at the T-invariant points $k_y = 0$ and $k_y = \infty$ [38].

Topological phase transition.—Figure 2 demonstrates that the stripe region undergoes a topological phase transition for material parameters in the range of recent experiments [24,30,31]. We obtain our results numerically using a tight-binding approximation of the effective Hamiltonian (4) [38,64].

We first discuss the T-symmetric case (left panels in Fig. 2). Starting from the topologically trivial regime ($W_{\mathbb{Z}} = 0$), one can identify a first phase transition at Zeeman energy $E_{Z,cr} \sim 120\ \mu$eV [$W_{\mathbb{Z}} = 0 \to 1$, Fig. 2(a)]. For a g factor of about 10 [30], this requires a magnetic field of ~200 mT, much lower than the critical fields in Al thin films [65]. At first sight, it may be surprising that the critical Zeeman energy $E_{Z,\rm cr}$ is smaller than the induced superconducting gap Γ under the superconducting top layers. The reason is that the Andreev bound states in the stripe experience the pairing potential only where they penetrate into the proximitized region and, as a consequence, the effective gap is smaller than Γ.

In agreement with the change in $W_{\mathbb{Z}}$, a pair of states comes close to zero energy around $E_Z = E_{Z,\rm cr}$ [Fig. 2(b)]. The wave functions of these states are localized at the ends of the stripe [Fig. 1(b)], and, because of the finite length of the stripe, their energies oscillate around zero [Fig. 2(c)]. From Fig. 2(b), we extract an energy gap to excited states—the topological energy gap—of about 20 μeV, which corresponds to about 200 mK.

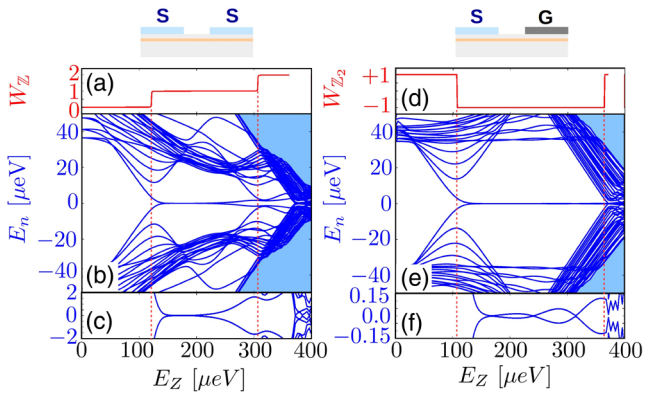

FIG. 2. Topological phase transition with increasing Zeeman field E_Z. The top pictograms illustrate the two cases studied here: on the left a symmetric device ($L_L = L_R$, class BDI) and on the right an asymmetric top-gated device ($L_R = 0$, class D). The upper panels show the topological invariant $W_{\mathbb{Z}}$ in (a) and $W_{\mathbb{Z}_2}$ in (d). The middle panels (b) and (e) depict the 50 lowest eigenenergies of $H_{\rm eff}(x, y)$ [Eq. (4)]. Higher excited states form a quasicontinuum in the light-blue shaded areas. Close-ups of the midgap-mode energies are shown in the lower panels (c) and (f). All parameters are as in Fig. 1(b).

A second phase transition takes place for $E_Z \sim 320\ \mu$eV [$W_{\mathbb{Z}} = 1 \to 2$, Fig. 2(a)], where, for a finite stripe length, a second pair of states approaches zero energy [Fig. 2(b)]. However, for the parameters chosen in Fig. 2, the states remain split in energy, because the $W_{\mathbb{Z}} = 2$ regime is close to the breakdown of the induced superconducting gap (at $E_Z = 2\Gamma \sim 360\ \mu$eV). By increasing the stripe width, one can reach the regime of two MBSs for lower E_Z [38]. To confirm the presence of the MBSs, one can probe the conductance of the stripe by two quantum point contacts [see Fig. 1(a)]. From numerical calculations, we find a zero-bias peak up to $2e^2/h$ [38,66–68].

For future applications for topological quantum-information processing, it is desirable to enhance the topological energy gap as much as possible. This can be achieved, for example, with an asymmetric device structure as depicted above Fig. 2(d): One replaces one of the superconducting layers by a top gate that creates a potential barrier for the electrons in the 2DEG underneath. We model this here by terminating the system at the right end of the stripe setting $L_R = 0$. The Hamiltonian is now in class D, since T symmetry is broken. The $\mathbb{Z}_2$ invariant $W_{\mathbb{Z}_2}$ indicates a phase transition around $E_Z \sim 120\ \mu$eV [$W_{\mathbb{Z}_2} = +1 \to -1$, Fig. 2(d)], and a single pair of states approaches zero energy [Fig. 2(e)]. Compared with the symmetric device, their energy splitting is much smaller [~0.1 μeV, Fig. 2(f)] and the topological gap is increased [~40 μeV, Fig. 2(e)]. An asymmetric device design thus seems promising for stabilizing MBSs.

Phase diagrams and topological gap.—To study the optimal conditions for observing MBSs in experiments more systematically, we next investigate the topological energy gap (see the caption of Fig. 3). Both the gap and the boundaries of the topological phases given by the zero-gap condition exhibit a nontrivial dependence on the different parameters (Fig. 3). Because of the finite-frequency and finite-size effects, the actual topological gap may be smaller, but by comparing with transport calculations (including both effects) we find only a small reduction [38].

We first focus on the case with inversion symmetry [Figs. 3(a)–3(c)]. The phase-transition point depends on the spin-orbit coupling α [Fig. 3(a)]; however, a change in α can be compensated by a shift of the electrochemical potential $\mu \to \mu + m^*\alpha^2/2$ [61]. By contrast, the topological gap depends in a nontrivial way on α: It becomes maximal around $\alpha \approx 1.2 \times 10^{-4}c$, close to experimental values [24], and is strongly suppressed for $\alpha > 2 \times 10^{-4}c$ for the experimentally relevant parameters used in Fig. 3(a) for fixed μ. From Fig. 3(b), we see that it is crucial to tune the electrochemical potential near zero if no phase bias is applied, which requires a strong gate coupling, similar to the situation for nanowires [35,36]. Finally, we find that a stripe width L_M of around 200 nm is optimal for a large topological gap [Fig. 3(c)].

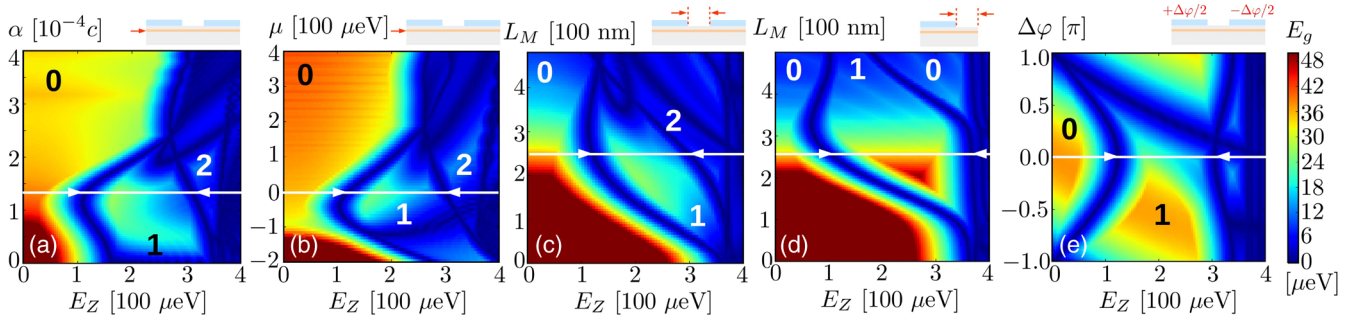

FIG. 3. Enhancing the topological energy gap defined by $E_g \equiv \min_{n,k_y}|E_n(k_y)|$, where $E_n(k_y)$ are the eigenenergies of $H_{\rm eff}(x, -i\partial_y \to k_y)$ [see Eq. (4)]. The gap is shown as a function of the Zeeman energy E_Z and (a) the spin-orbit velocity α, (b) the electrochemical potential μ, (c),(d) the width of the stripe L_M for a symmetric and asymmetric device, respectively, and (e) the phase difference $\varphi_L = -\varphi_R = \Delta\varphi/2$. We use $N_x = 300$ lattice points in (a), (b), and (e) but a finer resolution of $N_x = 3/2(L_L + L_M + L_R)$[nm] for (c) and (d). If not varied, all parameters are as in Fig. 1(b). The color scale is cut off at 50 μeV to enhance the contrast inside the regimes with a single MBS (we inserted the number of MBSs, marked phase-separation lines with white arrows, and indicated the parameters used in all other plots by white lines). We use absolute units, since various energy scales (Γ, Δ, μ, $m^*\alpha^2$) are in the same range and different combinations of them can govern the physics in the different regimes plotted.

As mentioned before, breaking the generalized T symmetry can further increase the topological gap. For example, the asymmetric, gated device [Fig. 3(d)] exhibits a topological gap that can be larger by a factor of up to 2. However, the gap can also be manipulated without breaking the generalized T symmetry in a phase-biased device [Fig. 3(e)]. Depending on the sign of the phase bias $\Delta\varphi$, the direction of the supercurrent is reversed, which through the spin-orbit term $i\alpha\sigma_y\partial_x$ affects the spectrum differently for a nonzero Zeeman term. This can both increase and decrease the gap, which could be used to determine the sign of α experimentally. Second, for both gating and phase bias, the regime of MBSs can be reached for smaller Zeeman energies [see $L_M \approx 300$ nm in Fig. 3(d) and $\Delta\varphi \approx -\pi$ in Fig. 3(e)].

Electrical control for MBS networks.—The above-mentioned sensitivity of the phase-transition point suggests the possibility to control the coupling of the MBSs electrically. To illustrate this, we assume that the nearby top gate creates a triangular confining potential for the MBSs [Figs. 4(a) and 4(b)]. By increasing the potential drop across the stripe by lowering V_g, the MBSs can be tuned from localized boundary modes [Fig. 4(d)] at zero energy into modes at finite energy and delocalized along the stripe [Fig. 4(c)]. Controlling the MBS coupling with a gate can be used for the initialization and readout of the MBSs also in larger networks of MBS stripes. Readout requires a way to detect the fermion parity of the MBSs, which can be achieved by charge detection [69], possibly using an auxiliary quantum dot [70].

To implement a qubit in a 2DEG structure, one can segment the MBS stripe into two parts using a finger gate [Fig. 4(e)]. Tuning this gate controls the coupling of the MBSs in the middle (indicated by crosses), which could be used to carry out fusion-rule and coherence-test experiments [22,23]. Finally, in order to realize braiding of MBSs similar to Refs. [18,20,22,23], one needs to couple three MBSs. Our numerical simulations indicate [38] that the topological phase is stable against a rotation of the magnetic field of about 10° away from the stripe direction. To keep the stripes in parallel, we suggest a "tuning-fork" design [Fig. 4(f)] instead of a T-junction structure usually considered for braiding.

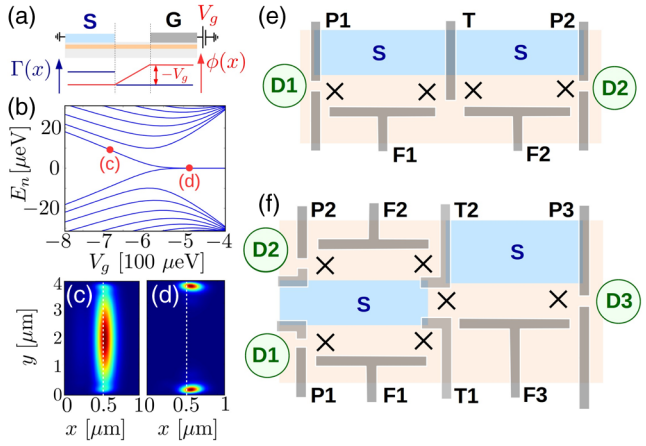

FIG. 4. Electrically controlled manipulation of MBSs in 2DEG devices. (a) Sketch of a MBS stripe whose width is controlled by a linear voltage drop tuned by a top gate (G) with (b) the corresponding low-energy spectrum. Below, we show the probability density $P(n_x, n_y)$ for the state closest to zero energy when the MBSs are (c) coupled and (d) uncoupled. We use $N_x = N_y = 150$ lattice points; all other parameters are as in Fig. 1(b). (e) By segmenting a MBS stripe into two parts using a gate (T), one could implement a qubit consisting of four MBSs (denoted by crosses). The intraisland coupling of the MBSs could be tuned by fusion gates ($F1$) and ($F2$) and the interisland coupling by the tunneling gate (T). For readout, the two gates ($P1$) and ($P2$) allow for coupling to two detectors ($D1$) and ($D2$). (f) Braiding setup with two gates ($T1$) and ($T2$) controlling the tunnel coupling between the three center MBSs.

Conclusion and outlook.—We have shown that 2DEG structures with strong spin-orbit coupling, proximity-induced superconductivity, and magnetic fields provide an alternative platform hosting MBSs that is readily available in the lab. A phase bias generated, e.g., by a supercurrent or a gate electrode allows us to move the phase-transition point *in situ* and to couple the MBSs by electrical means. Together with the technological advantage of flexible top-down fabrication of 2DEG structures, this might open the door for larger MBS networks. Recently, a preprint on a similar device appeared [61]. Differences are due to different parameter choices [38].

We acknowledge stimulating discussions with M. Kjaergaard, P. Kotetes, C. M. Marcus, F. Nichele, A. Stern, and H. J. Suominen and support from the Crafoord Foundation (M. L. and M. H.), the Swedish Research Council (M. L.), and The Danish National Research Foundation. Computational resources were partly provided by the Swedish National Infrastructure for Computing (SNIC) through Lunarc, the Center for Scientific and Technical Computing at Lund University.

[1] J. Alicea, Rep. Prog. Phys. **75**, 076501 (2012).
[2] M. Leijnse and K. Flensberg, Semicond. Sci. Technol. **27**, 124003 (2012).
[3] C. W. J. Beenakker, Annu. Rev. Condens. Matter Phys. **4**, 113 (2013).
[4] T. D. Stanescu and S. Tewari, J. Phys. Condens. Matter **25**, 233201 (2013).
[5] S. Bravyi and A. Kitaev, Ann. Phys. (Amsterdam) **298**, 210 (2002).
[6] S. Bravyi and A. Kitaev, Phys. Rev. A **71**, 022316 (2005).
[7] M. H. Freedman, A. Kitaev, M. J. Larsen, and Z. Wang, Bull. Am. Math. Soc. **40**, 31 (2003).
[8] V. Mourik, K. Zuo, S. M. Frolov, S. R. Plissard, E. P. A. M. Bakkers, and L. P. Kouwenhoven, Science **336**, 1003 (2012).
[9] A. Das, Y. Ronen, Y. Most, Y. Oreg, M. Heiblum, and H. Shtrikman, Nat. Phys. **8**, 887 (2012).
[10] A. D. K. Finck, D. J. Van Harlingen, P. K. Mohseni, K. Jung, and X. Li, Phys. Rev. Lett. **110**, 126406 (2013).
[11] L. P. Rokhinson, X. Liu, and J. K. Furdyna, Nat. Phys. **8**, 795 (2012).
[12] M. T. Deng, C. L. Yu, G. Y. Huang, M. Larsson, P. Caroff, and H. Q. Xu, Nano Lett. **12**, 6414 (2012).
[13] S. M. Albrecht, A. P. Higginbotham, M. Madsen, F. Kuemmeth, T. S. Jespersen, J. Nyg, P. Krogstrup, and C. M. Marcus, Nature (London) **531**, 206 (2016).
[14] H. Zhang *et al.*, arXiv:1603.04069.
[15] J. R. Williams, A. J. Bestwick, P. Gallagher, S. S. Hong, Y. Cui, A. S. Bleich, J. G. Analytis, I. R. Fisher, and D. Goldhaber-Gordon, Phys. Rev. Lett. **109**, 056803 (2012).
[16] S. Nadj-Perge, I. K. Drozdov, J. Li, H. Chen, S. Jeon, J. Seo, A. H. MacDonald, B. A. Bernevig, and A. Yazdani, Science **346**, 602 (2014).
[17] M. Ruby, F. Pientka, Y. Peng, F. von Oppen, B. W. Heinrich, and K. J. Franke, Phys. Rev. Lett. **115**, 197204 (2015).
[18] J. D. Sau, D. J. Clarke, and S. Tewari, Phys. Rev. B **84**, 094505 (2011).
[19] K. Flensberg, Phys. Rev. Lett. **106**, 090503 (2011).
[20] T. Hyart, B. van Heck, I. C. Fulga, M. Burrello, A. R. Akhmerov, and C. W. J. Beenakker, Phys. Rev. B **88**, 035121 (2013).
[21] J. Li, T. Neupert, B. A. Bernevig, and A. Yazdani, Nat. Commun. **7**, 12297 (2016).
[22] D. Aasen *et al.*, Phys. Rev. X **6**, 031016 (2016).
[23] M. Hell, J. Danon, K. Flensberg, and M. Leijnse, Phys. Rev. B **94**, 035424 (2016).
[24] J. Shabani *et al.*, Phys. Rev. B **93**, 155402 (2016).
[25] T. Schäpers, *Superconductor/Semiconductor Junctions* (Springer Science, New York, 2001), Vol. 174.
[26] A. Chrestin and U. Merkt, Appl. Phys. Lett. **70**, 3149 (1997).
[27] A. Chrestin, R. Kürsten, K. Biedermann, T. Matsuyama, and U. Merkt, Superlattices Microstruct. **25**, 711 (1999).
[28] H. Takayanagi, T. Akazaki, and J. Nitta, Phys. Rev. Lett. **75**, 3533 (1995).
[29] T. Bauch, E. Hürfeld, V. M. Krasnov, P. Delsing, H. Takayanagi, and T. Akazaki, Phys. Rev. B **71**, 174502 (2005).
[30] M. Kjaergaard *et al.*, Nat. Commun. **7**, 12841 (2016).
[31] M. Kjaergaard, H. J. Suominen, M. P. Nowak, A. R. Akhmerov, C. J. Shabani, C. J. Palmstrøm, F. Nichele, and C. M. Marcus, arXiv:1607.04164.
[32] H. Suominen, J. Danon, M. Kjaergaard, K. Flensberg, J. Shabani, C. Palmstrøm, F. Nichele, and C. Marcus, Phys. Rev. B **95**, 035307 (2017).
[33] J. D. Sau, R. M. Lutchyn, S. Tewari, and S. Das Sarma, Phys. Rev. Lett. **104**, 040502 (2010).
[34] J. Alicea, Phys. Rev. B **81**, 125318 (2010).
[35] R. M. Lutchyn, J. D. Sau, and S. Das Sarma, Phys. Rev. Lett. **105**, 077001 (2010).
[36] Y. Oreg, G. Refael, and F. von Oppen, Phys. Rev. Lett. **105**, 177002 (2010).
[37] N. Sedlmayr and C. Bena, Phys. Rev. B **92**, 115115 (2015).
[38] See Supplemental Material at http://link.aps.org/supplemental/10.1103/PhysRevLett.118.107701 for details on our numerical approach and results on transport spectra. We also discuss the magnetic field angle dependence of the topological gap and compare our results to that of Ref. [61]. The supplemental material includes Refs. [39–48].
[39] T. D. Stanescu, R. M. Lutchyn, and S. Das Sarma, Phys. Rev. B **84**, 144522 (2011).
[40] K. T. Law, P. A. Lee, and T. K. Ng, Phys. Rev. Lett. **103**, 237001 (2009).
[41] K. Flensberg, Phys. Rev. B **82**, 180516 (2010).
[42] A. Golub and B. Horovitz, Phys. Rev. B **83**, 153415 (2011).
[43] M. Wimmer, A. R. Akhmerov, J. P. Dahlhaus, and C. W. J. Beenakker, New J. Phys. **13**, 053016 (2011).
[44] B. Zocher and B. Rosenow, Phys. Rev. Lett. **111**, 036802 (2013).
[45] J. Liu, F.-C. Zhang, and K. T. Law, Phys. Rev. B **88**, 064509 (2013).
[46] C. W. J. Beenakker, Rev. Mod. Phys. **87**, 1037 (2015).

[47] I. L. Aleiner, P. W. Brouwer, and L. I. Glazman, Phys. Rep. **358**, 309 (2002).
[48] G. B. Lesovik, A. L. Fauch'ere, and G. Blatter, Phys. Rev. B **55**, 3146 (1997).
[49] J. D. Sau, R. M. Lutchyn, S. Tewari, and S. Das Sarma, Phys. Rev. B **82**, 094522 (2010).
[50] T. D. Stanescu, J. D. Sau, R. M. Lutchyn, and S. Das Sarma, Phys. Rev. B **81**, 241310 (2010).
[51] E. B. Hansen, J. Danon, and K. Flensberg, Phys. Rev. B **93**, 094501 (2016).
[52] R. Wakatsuki, M. Ezawa, and N. Nagaosa, Phys. Rev. B **89**, 174514 (2014).
[53] P. Kotetes, Phys. Rev. B **92**, 014514 (2015).
[54] R. M. Lutchyn, T. D. Stanescu, and S. Das Sarma, Phys. Rev. Lett. **106**, 127001 (2011).
[55] Z. Wang and B. Yan, J. Phys. Condens. Matter **25**, 155601 (2013).
[56] J. C. Budich and B. Trauzettel, New J. Phys. **15**, 065006 (2013).
[57] C. Wang *et al.*, Nat. Commun. **5**, 5836 (2014).
[58] A. Altland and M. R. Zirnbauer, Phys. Rev. B **55**, 1142 (1997).
[59] S. Ryu, A. P. Schnyder, A. Furusaki, and A. W. W. Ludwig, New J. Phys. **12**, 065010 (2010).
[60] The time-reversal operator and the particle-hole conjugation operator are not unique, since H_{eff} has an additional unitary symmetry $U = I_y\sigma_y$, where I_y is the reflection operator in the y direction.
[61] F. Pientka, A. Keselman, E. Berg, A. Yacoby, A. Stern, and B. I. Halperin, arXiv:1609.09482.
[62] S. Tewari and J. D. Sau, Phys. Rev. Lett. **109**, 150408 (2012).
[63] A. Y. Kitaev, Sov. Phys. Usp. **44**, 131 (2001).
[64] D. Ferry and S. M. Goodnick, *Transport in Nanostructures* (Cambridge University Press, Cambridge, England, 1997), Vol. 6.
[65] P. M. Tedrow and R. Meservey, Phys. Rev. B **25**, 171 (1982).
[66] C. J. Bolech and E. Demler, Phys. Rev. Lett. **98**, 237002 (2007).
[67] J. Nilsson, A. R. Akhmerov, and C. W. J. Beenakker, Phys. Rev. Lett. **101**, 120403 (2008).
[68] S. Tewari, C. Zhang, S. Das Sarma, C. Nayak, and D.-H. Lee, Phys. Rev. Lett. **100**, 027001 (2008).
[69] G. Ben-Shach, A. Haim, I. Appelbaum, Y. Oreg, A. Yacoby, and B. I. Halperin, Phys. Rev. B **91**, 045403 (2015).
[70] K. Gharavi, D. Hoving, and J. Baugh, Phys. Rev. B **94**, 155417 (2016).